

1 GSTZ1 sensitizes hepatocellular carcinoma cells to sorafenib-induced

2 ferroptosis via inhibition of NRF2/GPX4 axis

3 **Running title: GSTZ1 sensitizes HCC to sorafenib-induced ferroptosis**

4 Qiujie Wang^{1,*}, Bin Cheng^{1,*}, Qiang Xue^{2,*}, Qingzhu Gao¹, Ailong Huang^{1,†},

5 Kai Wang^{1, #}, Ni Tang^{1, #}

6 ¹Key Laboratory of Molecular Biology for Infectious Diseases (Ministry of
7 Education), Institute for Viral Hepatitis, Department of Infectious Diseases, The
8 Second Affiliated Hospital, Chongqing Medical University, Chongqing, China

²Department of Hepatobiliary Surgery, The Second Affiliated Hospital of Chongqing Medical University, Chongqing, China

11 *These authors contributed equally to this work.

12 **#Correspondence:** Ailong Huang, Kai Wang, Ni Tang, Key Laboratory of

13 Molecular Biology for Infectious Diseases (Ministry of Education), Institute for
14 Viral Hepatitis, Department of Infectious Diseases, The Second Affiliated
15 Hospital, Chongqing Medical University, Chongqing, China. Phone:

16 86-23-68486780, Fax: 86-23-68486780, E-mail: nitang@cqmu.edu.

17 ahuang@cqmu.edu.cn (A.L.H.), wangkai@cqmu.edu.cn (K.W.)

19

66 *The author's introduction*

21

22 **Abstract**

23 Increasing evidence supports that ferroptosis plays an important role in tumor growth
24 inhibition. Sorafenib, originally identified as an inhibitor of multiple oncogenic kinases,
25 has been shown to induce ferroptosis in hepatocellular carcinoma (HCC). However,
26 some hepatoma cell lines are less sensitive to sorafenib-induced ferroptotic cell death.
27 Glutathione S-transferase zeta 1 (GSTZ1), an enzyme in the catabolism of
28 phenylalanine, has been found to negatively regulate the master regulator of cellular
29 redox homeostasis nuclear factor erythroid 2-related factor 2 (NRF2). This study
30 aimed to investigate the role of GSTZ1 in sorafenib-induced ferroptosis in HCC cell
31 lines and determine the involved molecular mechanisms. Mechanistically, GSTZ1
32 depletion enhanced the activation of the NRF2 pathway and increased the glutathione
33 peroxidase 4 (GPX4) level, thereby suppressing sorafenib-induced ferroptosis. The
34 combination of sorafenib and RSL3, a GPX4 inhibitor, significantly inhibited GSTZ1
35 deficient cell viability and promoted ferroptosis, accompanied with ectopic increases
36 of iron and lipid peroxides. An *in vivo* experiment showed that the combination of
37 sorafenib and RSL3 had a synergic therapeutic effect on HCC progression in *Gstz1*^{-/-}
38 mice. In conclusion, GSTZ1 was significantly downregulated in sorafenib resistant
39 hepatoma cells. GSTZ1 enhanced sorafenib-induced ferroptosis by inhibiting the
40 NRF2/GPX4 axis in HCC cells. GSTZ1 deficiency was resistant to sorafenib-induced
41 ferroptosis and is, therefore, a potential therapeutic approach for treating HCC by
42 synergizing sorafenib and RSL3 to induce ferroptosis.

43

44 **Introduction**

45 Hepatocellular carcinoma (HCC) is the fourth leading cause of cancer-related
46 death worldwide ¹. In the early stages of HCC, curative treatment can be
47 achieved with tumor ablation, resection, or liver transplantation ². However,
48 majority of HCC patients are already in the middle-late stage when diagnosed;
49 thus, the optimal period for curative treatment is missed. Sorafenib, a
50 multi-target kinase inhibitor, has been confirmed to prolong the survival of
51 advanced HCC patients to 6.5 months in phase III trial ³. Thus, it has been
52 approved by the Food and Drug Agency as a first-line treatment for advanced
53 HCC. However, several patients with advanced HCC have limited survival
54 benefit due to acquired resistance to sorafenib, leading to a high recurrence
55 rate ⁴. Therefore, the mechanism of sorafenib resistance needs to be explored,
56 and new molecular targets should be identified.

57

58 Ferroptosis is a newly described programmed form of cell death characterized
59 by iron-dependent accumulation of lipid peroxides to lethal amounts, different
60 from the traditional cell death forms of apoptosis, necroptosis, and autophagy ⁵.
61 Growing evidence indicates that ferroptosis can be induced by the inhibition of
62 cystine/glutamate transporter (SLC7A11/xCT) activity, downregulation of
63 glutathione peroxidase 4 (GPX4), and accumulation of iron and lipid reactive
64 oxygen species (ROS) ⁶⁻⁸. Recent reports have shown that sorafenib could
65 induce ferroptosis; thus, targeting ferroptosis to improve sorafenib therapy

66 might be a new promising strategy for HCC treatment ^{9–11}.

67

68 Glutathione S-transferases (GSTs) is a class of phase II detoxification
69 enzymes that catalyze the conjugation of glutathione (GSH) to endogenous or
70 exogenous electrophilic compounds ¹². GSTs, including GSTM and GSTP ^{13–15},

71 are involved in the development of chemotherapy resistance ^{16,17}. Glutathione
72 S-transferase zeta 1 (GSTZ1) is an important member of the GST superfamily.

73 It participates in the catabolism of phenylalanine/tyrosine and catalyzes the
74 isomerization of maleylacetoacetate to fumarylacetoacetate ¹⁸. We previously

75 found that GSTZ1 was poorly expressed in HCC, and GSTZ1 deficiency could
76 lead to metabolite succinylacetone accumulation and thereby activate the
77 NRF2 signaling pathway ^{19,20}. Considering the importance of GSTZ1 in the
78 development and progression of HCC, GSTZ1 may be an anticancer hallmark
79 for sorafenib resistance in HCC. Therefore, it is crucial to investigate the role of
80 GSTZ1 in chemotherapeutic resistance and elucidate underlying mechanisms.

81 In the present study, we investigated the role of GSTZ1 in sorafenib-induced
82 ferroptosis in HCC cell lines *in vitro* and in Gstz1-knockout mice *in vivo*, and
83 determined the involved molecular mechanisms. Our study not only identify a
84 novel mechanism of sorafenib resistance but also suggest a new link between
85 GSTZ1 and ferroptosis.

86

87 **Results**

88 **GSTZ1 is downregulated in sorafenib-resistant HCC**

89 To investigate the molecular mechanism of sorafenib resistance in HCC, we
90 generated sorafenib-resistant (SR) HCC cell lines *in vitro*. Resistance was
91 achieved by gradually increasing the concentration of sorafenib in the medium
92 over repeated passages ²¹. Finally, resistant HepG2 and SNU449 cell lines
93 were established. We confirmed the acquired resistance of these resistant
94 cells named HepG2-SR and SUN449-SR toward sorafenib by comparing to
95 the parental cells. The half maximal inhibitory concentrations (IC₅₀) of
96 HepG2-SR and SNU449-SR cells to sorafenib were 2-3 times higher than that
97 of the parental cells at 17.09 μ M and 15.43 μ M respectively (Fig. 1A). In
98 addition, we evaluated the cell viability of sensitive and resistant cells treated
99 with sorafenib over a series of time points or at different concentrations for 24h
100 and found that the SR cells became less sensitive to sorafenib (Fig. 1B-C). To
101 verify the role of GSTZ1 in sorafenib-resistant HCC, we comprehensively
102 analyzed the expression levels of GSTZ1 in HepG2 cells and HepG2 cells
103 resistant to sorafenib in GSE62813 databases. The results showed that
104 GSTZ1 was significantly downregulated in SR cells (Fig. 1D). Subsequently,
105 we further validated the low levels of GSTZ1 expression in SR cell lines via
106 quantitative reverse-transcription polymerase chain reaction (qRT-PCR) and
107 Western blotting (Fig. 1E-F). Together, these data indicate that GSTZ1 may
108 play a negative role in mediating the resistance to sorafenib in HCC cells.

109

110 **GSTZ1 Knockout promotes sorafenib resistance in HCC**

111 To further evaluate whether GSTZ1 is related to sorafenib-resistance in HCC,

112 we found that overexpression of GSTZ1 through an adenovirus system ^{19,20}

113 increased the sensitivity of HCC cells to sorafenib and inhibited cell

114 proliferation via morphological observation. Conversely, knockout of GSTZ1 in

115 HepG2 and SNU449 cells via the CRISPR-Cas9 system ^{19,20} decreased the

116 drug sensitivity and weakened the growth inhibition effect of sorafenib (Fig.

117 2A-B). Next, we analyzed the cell viability of GSTZ1 overexpression (OE) and

118 knockout (KO) cells treated with sorafenib over a series of time points or at

119 different concentrations for 24 h by cell growth curve. As expected, GSTZ1

120 overexpression significantly enhanced the sensitivity of HCC cell lines to

121 sorafenib (Fig. 2C-D). No surprisingly, the IC₅₀ value of GSTZ1-OE cells was

122 decreased compared to that of the control groups, whereas the IC₅₀ value of

123 GSTZ1-KO groups was increased (Fig. 2E-F). Taken all together, our results

124 showed that GSTZ1 deficiency enhanced sorafenib resistance in HCC.

125

126 **GSTZ1 overexpression enhances sorafenib-induced ferroptosis in HCC**

127 Recent studies indicate that ferroptosis plays a key role in the

128 chemoresistance of human cancers ²²⁻²⁴. We confirmed that sorafenib-induced

129 cell death in HCC cell lines was blocked by ferrostatin-1 (Fer-1, an inhibitor of

130 ferroptosis), deferoxamine (DFO, an iron chelator), and N-acetyl-L-cysteine

131 (NAC, an antioxidant), but not by baflomycin A1 (Baf-A1, an inhibitor of
132 autophagy), ZVAD-FMK, and necrosulfonamide (Nec, an inhibitor of
133 necroptosis). This suggested that ferroptosis, rather than apoptosis, is
134 essential for sorafenib-induced cell death in HCC (Supplementary Fig. 1A),
135 consistent with previous studies ^{11,25,26}. To determine whether GSTZ1 played a
136 role in ferroptosis to reduce sorafenib resistance in HCC, transmission electron
137 microscopy (TEM) was used to observe the morphological changes in
138 sorafenib-induced HCC cells with or without GSTZ1 depletion. GSTZ1-OE
139 cells treated with sorafenib displayed smaller mitochondria, diminished or
140 vanished mitochondria crista, and condensed mitochondrial membrane
141 densities compared to parental cells, whereas GSTZ1-KO alleviated the
142 abnormalities of mitochondrial morphology and cell death induced by sorafenib
143 (Fig. 3A). To further verify this observation, we measured ROS, iron and lipid
144 peroxidation levels, which are the primary cause of ferroptosis²⁷, after
145 interference with GSTZ1 expression. Results showed that GSTZ1
146 overexpression significantly increased ROS, iron, and MDA level accumulation
147 in sorafenib-induced HCC cell lines (Fig. 3B-D and Supplementary Fig. 1B-C),
148 whereas GSTZ1 knockout decreased their levels. In addition, we assessed
149 mRNA and protein expression levels of ferroptosis-associated genes. Results
150 showed that GSTZ1-OE decreased the expression levels of ferroptosis-related
151 genes in sorafenib or erastin (an inducer of ferroptosis)-induced hepatoma
152 cells, including *GPX4*, *FTL*, and *SLC7A11*. In contrast, GSTZ1-KO increased

153 the levels of these above genes (Fig. 3E-G and Supplementary Fig. 1D-E).

154 Interestingly, ferroptosis-associated genes were also enhanced in HepG2-SR

155 and SNU449-SR cells (Fig. 4A-B), which had relatively lower levels of GSTZ1

156 than the parental cells. Meanwhile, GSTZ1 overexpression in drug-resistant

157 cells reduced the levels of ferroptosis-related genes (Fig. 4C), increased the

158 accumulation of iron and MDA levels, and enhanced the inhibition of sorafenib

159 to resistant cells (Fig. 4D-F), consistent with the sorafenib-sensitive cells.

160 To further identify the role of ferroptosis in sorafenib resistance caused by

161 GSTZ1 deficiency, we examined the curative effects of sorafenib by

162 intervention of ferroptosis. We observed that ferrostatin-1 inhibited

163 sorafenib-induced GSTZ1-OE cell death, whereas erastin promoted

164 GSTZ1-KO cell death (Fig. 4G). These results suggested that GSTZ1

165 increased the sensitivity of hepatoma cells to sorafenib by inducing ferroptosis.

166

167 **GSTZ1 sensitizes hepatoma cells to sorafenib-induced ferroptosis**

168 **through the NRF2 signaling pathway**

169 Previous studies have shown that GSTZ1 deficiency activated NRF2 pathway

170 ^{19,20}. Activation of NRF2 pathway plays a critical role in protecting HCC cells

171 against sorafenib-induced ferroptosis ²⁶. To verify whether GSTZ1 regulated

172 sorafenib-induced ferroptosis through the NRF2 signaling pathway, we

173 blocked the NRF2 pathway using brusatol (an inhibitor of NRF2) or

174 Flag-tagged Kelch-like ECH-associated protein 1 (KEAP1) ²⁸ (an cytosolic

175 inhibitor of NRF2) in GSTZ1-KO cells and observed the characteristic
176 indicators related to ferroptosis, including MDA, iron, ROS, and 4-HNE levels.
177 Unexpectedly, the results demonstrated that NRF2 inhibition significantly
178 increased the accumulation of these indicators in GSTZ1-KO cells (Fig. 5A-D
179 right, Fig. 5E-F bottom, and Supplementary Fig. 2A-C bottom), whereas NRF2
180 activation using tertiary butylhydroquinone (tBHQ, an activator of NRF2) and
181 Myc-tagged NRF2 yielded opposite results in GSTZ1-OE cells (Fig. 5A-D left,
182 Fig. 5E-F top and Supplementary Fig. 2A-C top). Moreover, the morphological
183 images also indicated that NRF2 inhibition increased the efficiency of
184 sorafenib for growth inhibition in GSTZ1-depleted HCCs, whereas NRF2
185 activation decreased that in GSTZ1-OE cells (Fig. 6A). Importantly, the protein
186 levels of ferroptosis-related genes were changed accordingly in GSTZ1-OE
187 and -KO cells when treated with tBHQ or brusatol via Western blotting (Fig. 6B
188 and Supplementary Fig. 2D). The above data suggested that GSTZ1 depletion
189 alleviated sorafenib-induced ferroptosis via activation of the NRF2 pathway.
190 As GPX4 is involved in ferroptosis and a transcriptional target gene of NRF2
191 ^{29,30}, we utilized RSL3 to further examine whether ferroptosis is involved in the
192 sensitivity of HCC cells to sorafenib. Interestingly, GPX4 inactivation enhanced
193 sorafenib-induced ferroptosis and inhibited cell growth in GSTZ1-KO (Fig.
194 6C-E) and SR cells (Fig. 6F-H). Collectively, these findings indicated that the
195 inhibition of NRF2 could markedly sensitize GSTZ1-deficient hepatoma cells to
196 sorafenib treatment. Furthermore, we further examined targeting GPX4 could

197 also improve the response of hepatoma cells to sorafenib.

198

199 **RSL3 enhances the anticancer activity of sorafenib in *Gstz1*^{-/-} mice**

200 To further investigated the role of GSTZ1 in mediating sorafenib resistance in

201 HCC progression *in vivo*, we established the mouse model of liver cancer

202 induced by DEN/CCl₄ as our previous induction method²⁰ and drug

203 administration with three regimens: DMSO, sorafenib (30mg/kg, every 2 days

204 for 4 weeks), RSL3 (10mg/kg, every 2 days for 4 weeks) (Fig. 7A). Compared

205 with wild type (WT) mice, *Gstz1* knockout significantly reduced the inhibitory

206 effects of sorafenib treatment *in vivo* than that in WT mice, as indicated by the

207 increased tumor sizes and number of tumor nodules and higher level of

208 alanine aminotransferase (ALT) in serum (Fig. 7B-E). Moreover, sorafenib

209 combined with RSL3 had a more significant protective effect on tumorigenesis

210 in *Gstz1*^{-/-} mice than sorafenib alone. To substantiate the role of GSTZ1 in

211 regulating ferroptosis-mediated sorafenib resistance *in vivo*, we detected the

212 levels of iron, 4-HNE modification, MDA, ROS and ferroptosis-associated gene

213 expression mRNA and protein in the liver tumor tissues. Consistent with the

214 results *in vitro*, *Gstz1* knockout decreased the sensitivity of HCC to sorafenib

215 by weakening ferroptosis. Meanwhile, RSL3/sorafenib combination treatment

216 reduced drug resistance caused by GSTZ1 depletion (Fig. 7F-J and

217 Supplementary Fig. 3A). Furthermore, histological analysis indicated that the

218 cytoplasm and nuclei of liver tumors in the combination treatment groups

219 exhibited weaker immunoreactivity for GPX4 and Ki67 respectively than that in
220 sorafenib-alone groups. RSL3 significantly enhanced the inhibitory effects of
221 sorafenib on cell proliferation in *Gstz1*^{-/-} mice, which was highly consistent
222 with the in vitro results (Fig. 7K). These results indicate that targeting the
223 NRF2/GPX4 axis using RSL3 significantly enhances sorafenib-induced
224 ferroptosis and inhibits hepatocarcinogenesis *in vivo*.
225

226 **Discussion**

227 The incidence of HCC continues to increase globally, and HCC remains to
228 have high incidence and mortality rates³¹. Sorafenib resistance remains a
229 treatment challenge in HCC and leads to poor prognosis³². Therefore, the
230 comprehensive elucidation of the underlying mechanism of sorafenib
231 resistance in HCC may improve the curative effect of chemotherapy and guide
232 the clinical medication. Herein, we found that GSTZ1 depletion activated the
233 NRF2/GPX4 pathway and inhibited sorafenib-induced cell death, accompanied
234 by the compromised accumulation of iron level, lipid peroxidation, and
235 subsequent ferroptosis. Hence, blocking the NRF2/GPX4 pathway to enhance
236 the anticancer activity of sorafenib by inducing ferroptosis represents a
237 promising therapeutic strategy for the treatment of HCC (Fig. 8).

238

239 GSTs are phase II detoxification enzymes that play important roles in
240 protecting cellular macromolecules from both oxidative stress and
241 carcinogenic electrophiles³³. The major roles of GSTs in the detoxification of
242 xenobiotics predicts their important role in drug resistance. Tumor cells may
243 develop resistance to alkylating anticancer drugs by increasing the levels of
244 GSTs³⁴. Several subclasses in the GST family contribute to chemoresistance
245 in various cancers^{15,35-40}. GSTM1 was reported to be a predictive biomarker
246 for the efficacy of chemotherapy in breast cancer and ovarian cancer^{15,35}.
247 GSTP expression was also correlated with platinum drug chemosensitivity and

248 prognosis in ovarian cancer, pancreatic ductal adenocarcinoma, and lung
249 cancer³⁶⁻³⁹. As a member of the GST family, GSTZ1 plays a similar
250 detoxification role, but it is independently characterized as a
251 maleylacetoacetate isomerase (MAAI), which is essential for phenylalanine
252 metabolism¹⁸. We previously reported that GSTZ1 is downregulated in HCC,
253 leading to increased accumulation of the carcinogenic metabolite
254 succinylacetone and activation of the NRF2/IGFIR pathways through
255 inactivation of KEAP1¹⁹. The current study demonstrates that GSTZ1 is also
256 downregulated in sorafenib-resistant HCC cells. Furthermore, re-expression of
257 GSTZ1 enhances the sensitivity of HCC cells to sorafenib treatment, indicating
258 the negative role of GSTZ1 in sorafenib resistance.

259
260 Iron is an essential element for the synthesis of iron sulfur clusters, serving an
261 important role in numerous cellular processes⁴¹. Cancer cells exhibit a higher
262 dependence on iron than normal cells⁴², making them more susceptible to
263 iron-catalyzed necrosis. This form of cell death was first defined as ferroptosis
264 in 2012⁵, which characterized by the accumulation of lipid peroxidation
265 products and lethal ROS derived from iron metabolism^{6,27}. An increasing
266 number of small molecule compounds (e.g., erastin) or clinical drugs (e.g.,
267 sulfasalazine) has been found to induce ferroptosis by modulating iron
268 metabolism and enhancing the accumulation of lipid peroxidation^{6,43}. As a
269 homeostatic dysfunction of ferroptosis is believed to be an essential cause of

270 chemoresistance⁴⁴, it is crucial to explore how to enhance the sensitivity of
271 cancer cells to clinical chemotherapy drugs by triggering ferroptosis. In the
272 case, ferroptosis inducer erastin significantly enhances the anticancer activity
273 of cytarabine and doxorubicin in leukemia cells⁴⁵. It also reverses the
274 resistance of ovarian cancer cells to cisplatin⁴⁶. Multiple studies recently
275 verified that sorafenib plays an important role in inducing ferroptosis. Herein,
276 we found that GSTZ1 deficiency aggravated the resistance to
277 sorafenib-induced ferroptosis by preventing iron accumulation and lipid
278 peroxidation production and decreasing the ROS level. In contrast, GSTZ1
279 overexpression increased the sensitivity of HCC cells to sorafenib by
280 facilitating ferroptosis *in vitro*. Previous studies found that sorafenib-induced
281 hepatoma cell death is mainly dependent on triggering ferroptosis by inhibiting
282 of SLC7A11/xCT^{10,11,24}, and consistent findings were observed in this study.
283 As such, inducing ferroptosis may be a promising strategy for enhancing the
284 sensitivity of tumor cells to chemotherapy. Haloperidol, a sigma-1 receptor
285 (S1R) antagonist, promotes sorafenib-induced ferroptotic death by increasing
286 ROS accumulation⁴⁷. Meanwhile, metallothionein-1G silencing (MT-1G) was
287 reported to enhance the sensitivity of hepatoma cells to sorafenib by triggering
288 ferroptosis²⁴. Collectively, our findings and those of previous studies suggest
289 that ferroptosis plays an important role in the anti-tumor efficacy of sorafenib.
290 Further, our data indicated that GSTZ1 plays a positive regulatory role in
291 ferroptosis during sorafenib treatment.

292

293 Changes in certain metabolic pathways are also involved in the regulation of
294 cell sensitivity to ferroptosis, including coenzyme Q10 consumption ⁴⁸,
295 decreased intracellular reducer such as NAPDH ⁴⁹, and altered iron
296 metabolism ⁵⁰. Many components of the ferroptosis cascade are target genes
297 of the transcription factor NRF2, indicating the critical role of the NRF2
298 pathway in mediating ferroptotic response ^{29,30,51}. For example, the inhibition of
299 p62-Keap1-NRF2 pathway significantly enhanced the anticancer activity of
300 erastin and sorafenib by inducing ferroptosis in HCC cells *in vitro* and *in vivo*
301 [27]. Consistent with previous reports, our results demonstrated that GSTZ1
302 deficiency markedly reduces sorafenib-induced ferroptotic cell death by
303 increasing the level of NRF2 and ferroptosis-related genes including GPX4,
304 SLC7A11, and FTL. In contrast, pharmacological- or Keap1-mediated
305 inhibition of NRF2 increases the sensitivity of GSTZ1-deficient cells to
306 sorafenib by enhancing ferroptosis *in vitro*. Meanwhile, GPX4 is the only
307 reported enzyme that is capable of directly reducing complex phospholipid
308 hydroperoxides and is a downstream target gene of NRF2. Therefore,
309 targeting GPX4 is currently considered to be a crucial strategy for triggering
310 ferroptosis ^{7,44}. Mechanistically, we verified that GSTZ1 knockout inhibited
311 sorafenib-induced ferroptosis by activation of the NRF2/GPX4 axis *in vitro* and
312 *in vivo*. Moreover, targeting GPX4 using RSL3 in GSTZ1-knockout and
313 sorafenib-resistant HCC cells significantly increased iron accumulation, ROS

314 level, and lipid peroxidation production and enhanced sorafenib-induced
315 inhibition of cell proliferation. Importantly, GPX4 inhibition using RSL3 with
316 sorafenib therapy elicited a significant tumor regression in *Gstz1*^{-/-} mouse
317 models *in vivo*.

318

319 To our best knowledge, this is the first study to explore the role of GSTZ1 in
320 sorafenib resistance in HCC. Our findings provide new insights into the
321 molecular basis of the role of GSTZ1 in sorafenib resistance, and indicate that
322 sorafenib combined with RSL3 can synergistically overcome acquired
323 resistance to sorafenib and improve the anticancer efficacy of sorafenib in
324 HCC. Blocking the NRF2/GPX4 axis may have a therapeutic benefit in HCC
325 patients with GSTZ1 deficiency. Our findings also demonstrate the sensitizing
326 role of RSL3 for enhancing sorafenib effectiveness. Importantly, GSTZ1
327 deficiency was resistant to sorafenib-induced ferroptosis and is therefore a
328 potential therapeutic approach for treating HCC by synergizing sorafenib and
329 RSL3 to induce ferroptosis.

330

331 **Materials and Methods**

332 **Cell lines**

333 Human hepatoma cell lines SK-Hep1, HepG2 and SNU449 were directly
334 obtained from American Type Culture Collection (ATCC, VA, USA). Huh7 cells
335 were obtained from Cell Bank of the Chinese Academy of Sciences (Shanghai,
336 China). These cells were cultured in Dulbecco's modified Eagle's medium
337 (SK-Hep1, HepG2, Huh7) or RPMI 1640 medium (SNU449) supplemented
338 with 10% fetal bovine serum (FBS; Gibco, Rockville, MD, USA), 100units/mL
339 penicillin and 100mg/mL streptomycin in a humidified incubator at 37 °C
340 containing 5% CO₂.

341

342 **Reagents and antibodies**

343 Erastin (HY-15763), Ferrostatin-1 (HY-100579), Deferoxamine (HY-B0988)
344 and Necrosulfonamide (HY-100573) were purchased from MedChemExpress
345 (MCE; Shanghai, China). Sorafenib (S7397), ZVAD-FMK (S7023), Bafilomycin
346 A1 (S1413) and RSL3 (S8155) were obtained from Selleckchem (Houston, TX,
347 USA). N-acetyl-L-cysteine (NAC, S0077) was from Beyotime (Shanghai,
348 China). Brusatol (Bru, MB7292) was obtained from Meilunbio (Dalian, China).
349 Tertiary butylhydroquinone (tBHQ, 112941) was obtained from Sigma
350 (Shanghai, China). Antibodies raised against GPX4 (ab125066), NRF2
351 (ab62352), 4-HNE(ab46545), NQO1(ab34173) and β-actin (ab6276) were
352 obtained from Abcam (Cambridge, MA, USA), anti-SLC7A11 (NB300-318) was

353 from Novusbio (Centennial, CO, USA), anti-FTL (10727-1-AP) was from
354 Proteintech (Shanghai, China), and anti-GSTZ1 (GTX106109) was from
355 GeneTex (San Antonio, CA, USA).

356

357 **Generation of sorafenib-resistant cell lines**

358 To establish sorafenib-resistant cells, HepG2 and SNU449 cells were cultured
359 by exposing cells with sorafenib at 5% of IC50 concentration and the
360 concentration was gradually increased at 10% of IC50 until the maximum
361 tolerated doses (10 μ M) have been reached. Sorafenib-resistant cells
362 (HepG2-SR and SNU449-SR) were cultured continuously at 1 μ M
363 concentration of sorafenib to maintain the acquired resistance.

364

365 **Quantitative real-time polymerase chain reaction (qRT-PCR)**

366 Total RNA was isolated from HCC cell lines using TRIzol reagent (Invitrogen,
367 Rockville, MD, USA) according to the manufacturer's instructions. Purified
368 RNA samples were reverse-transcribed into cDNA using the PrimeScriptTM RT
369 Reagent Kit with gDNA Eraser (RR047A, TaKaRa, Tokyo, Japan).
370 Complementary DNA from cell samples was amplified with the specific primers
371 (Supplementary Table. 1). Briefly, Real-time qPCR was performed to quantity
372 mRNA levels, using the SYBR Green qPCR Master Mix (Bio-Rad, Hercules,
373 CA, USA) in accordance with the manufacturer's instructions. The objective
374 CT values were normalized to that of β -actin and relative mRNA expression

375 levels of genes were calculated using $2^{-\Delta\Delta Ct}$ method. Each sample was
376 analyzed in triplicate.

377

378 **Western blot analysis**

379 Protein samples from cells and animal tissues were lysed in Cell Lysis Buffer
380 (Beyotime Biotechnology, Jiangsu, China) containing 1mM of
381 phenylmethanesulfonyl fluoride (PMSF, Beyotime). The concentration of the
382 protein homogenates was measured using the BCA protein assay Kit (Dingguo,
383 Beijing, China). Equal volumes of protein samples were separated by
384 SDS-poly acrylamide gel electrophoresis and electro-transferred to PVDF
385 membranes (Millipore, Billerica, MA, USA). After blocked with 5% non-fat milk
386 dissolved in TBST (10mM Tris, 150 mM NaCl, and 0.1% Tween-20; pH 7.6),
387 for 2 h at room temperature, the membranes were incubated with the primary
388 antibodies overnight at 4 °C. Thereafter, membranes were incubated with the
389 secondary antibodies coupled to horseradish peroxidase (HRP) for 2 h at room
390 temperature. Protein bands were visualized with enhanced
391 Chemiluminescence substrate Kits (ECL, New Cell & Molecular Biotech Co,
392 Ltd, China).

393

394 **Transmission electron microscope assay**

395 Cells were collected and fixed with 2.5% glutaraldehyde. Subsequently, cells
396 were postfixed in 2% osmium tetroxide and dehydrated through a series of

397 graded ethyl alcohols. Samples were embedded in epoxy resin, sectioned, and
398 placed onto nickel mesh grids. The images were acquired using a Hitachi-7500
399 transmission electron microscope (Hitachi, Tokyo, Japan).

400

401 **Intracellular ROS measurements**

402 Cells were seeded on coverslips in a 12-well plate, and then treated with the
403 varying concentrations of test compound or drug. After 24 h, cells were
404 incubated at a final concentration of 5 μ M CellROX® Orange reagent (Life
405 Technologies, Carlsbad, USA) for 30 min at 37 °C, after which they were
406 washed, dyed with DAPI, mounted with Anti-fade Mounting Medium, and
407 immediately analyzed for fluorescence intensity under Leica Confocal
408 Microscope (TCS SP8, Germany) with a 40x objective lens.

409

410 **Measurement of total iron contents in hepatoma cells and liver tissues**

411 The iron concentration was assessed using the Iron Assay Kit (MAK025;
412 Sigma) according to the manufacturer's instructions. Briefly, tissues (10 mg) or
413 cells (2×10^6) were rapidly homogenized in 4-10 volumes of Iron Assay buffer.
414 Tissue or cell homogenates was centrifuged at 16,000 $\times g$ for 10 minutes at 4
415 °C and removed insoluble material. To measure total iron, add 1-50 μ L
416 samples to sample wells in a 96 well plate, bring the volume to 100 μ L per well
417 with Iron Assay Buffer and add 5 μ L Iron Reducer to each of the sample wells
418 to reduce Fe^{3+} to Fe^{2+} . And then samples were mixed using a horizontal

419 shaker and incubated at 25 °C for 30 minutes. Subsequently, 100 µL Iron
420 Probe were added and incubated the reaction for 1 hr at 25 °C. During each
421 incubation, the plate was protected from light. Thereafter, the absorbance was
422 detected at 593 nm using a microplate reader.

423

424 **Detection of malondialdehyde (MDA)**

425 Analysis of lipid peroxidation was assessed by quantification of MDA
426 concentration in cell lysates using a Lipid Peroxidation MDA Assay Kit (S0131)
427 obtained from Beyotime in accordance with the manufacturer's instructions.

428

429 **Cell growth curve and cell viability assay**

430 For cell growth curve analysis, cells were seeded at 1×10^4 cells/well in 96-well
431 microtiter plates with three replicate per group and cultured overnight at 37°C
432 in a humidified incubator containing 5% CO₂. The plate was scanned and
433 phase-contrast images were acquired after over a series of time points post
434 treatment, and then quantified time-lapse curves were plotted using IncuCyte
435 ZOOM software (Essen BioScience, Ann Arbor, MI, USA).

436 For cell viability assay, cells were seeded at 1,000 cells per well in 96-well
437 plates with fresh medium and analysed by using the Cell Counting Kit-8
438 (CCK-8) (CK04, Dojindo, Japan) according to the manufacturer's instructions.
439 The microplates were incubated at 37°C for additional 2 h. Absorbance was
440 read at 450 nm using a microplate reader (Thermo Fisher, USA).

441

442 **Half maximal inhibitory concentration assay (IC50)**

443 The cells were planted in 96-well plates with fresh medium at 1.0×10^4 cells per
444 well. The corresponding concentrations of drug were given to cells for 24 h
445 after the cultured plates were placed in a humidified incubator for 12 h. After 24
446 h, CCK-8 (Dojindo, Japan) was used to measure drug sensitivity at 450 nm
447 using a microplate reader (Thermo Fisher, USA) after incubating at 37 °C for
448 1–2 h.

449

450 **Animal experiments**

451 Heterozygous 129-*Gstz1*^{tm1Jmfc}/Cnbc mice (EM: 04481) were purchased from
452 the European Mouse Mutant Archive and were crossed to breed wild-type (WT)
453 and *Gstz1*^{-/-} mice. All mice were maintained under individual ventilation cages
454 conditions in the laboratory animal center of Chongqing Medical University. For
455 subsequent studies, mice were divided into five groups as follows: WT+DMSO
456 (control), WT+Sora, *Gstz1*^{-/-}+DMSO, *Gstz1*^{-/-}+Sora, and
457 *Gstz1*^{-/-}+Sora+RSL3. Each group included three male and three female mice.
458 At 2 weeks of age, all mice were administered an intraperitoneal injection of
459 diethylnitrosamine (DEN; Sigma, St. Louis, MO, USA) at a dose of 75 mg/kg.
460 At the third week, the mice were intraperitoneally administered carbon
461 tetrachloride (CCl₄; Macklin, Shanghai, China) at 2 ml/kg twice a week for 12
462 weeks. In the WT+Sora and *Gstz1*^{-/-}+Sora group, the mice at 22 weeks were

463 administered intraperitoneally sorafenib (30mg/kg) every 2 days for 4 weeks
464 until euthanasia. In the *Gstz1*^{-/-}+Sora+RSL3 group, in addition to sorafenib
465 administration as described above, the mice were injected intraperitoneally
466 with RSL3 (10mg/kg) every 2 days for 4 weeks at the same weeks. Body
467 weight of each mice was measured every week and retroorbital blood was
468 collected before sacrifice. All mice were euthanized at 26 weeks of age. The
469 liver weight and number of liver tumors were measured. Protein and mRNAs
470 levels of hepatic tumors were detected by Western blotting and qRT-PCR
471 analysis, respectively. The intrahepatic Iron and MDA levels were measured
472 with Iron Assay Kit and MDA Assay Kit, respectively. Samples of liver tumor
473 were collected for further study or fixed with 4% paraformaldehyde, embedded
474 in paraffin, and sectioned for hematoxylin-eosin staining (H&E) and
475 immunohistochemistry. All animal procedures were approved by the Research
476 Ethics Committee of Chongqing Medical University (reference number:
477 2017010).

478

479 **Statistical analysis**

480 All experiments were repeated independently with similar results at least three
481 times. Statistical analysis and data plotting were performed using GraphPad
482 Prism 7 (GraphPad Software, USA). All data were presented as mean \pm
483 standard deviation (SD) values. Unless mentioned otherwise, comparisons
484 between two groups were performed by Student's t-test, and Multiple-group

485 comparisons were performed by the one-way ANOVA analysis with Scheffe

486 post-hoc test. $p < 0.05$ was considered statistically significant.

487

488

489 **References**

- 490 1 Bray F, Ferlay J, Soerjomataram I, Siegel RL, Torre LA, Jemal A. Global
491 cancer statistics 2018: GLOBOCAN estimates of incidence and mortality
492 worldwide for 36 cancers in 185 countries. *CA: A Cancer Journal for Clinicians*
493 2018; **68**: 394–424.
- 494 2 Yang JD, Hainaut P, Gores GJ, Amadou A, Plymoth A, Roberts LR. A global
495 view of hepatocellular carcinoma: trends, risk, prevention and management.
496 *Nat Rev Gastroenterol Hepatol* 2019; **16**: 589–604.
- 497 3 Cheng A-L, Kang Y-K, Chen Z, Tsao C-J, Qin S, Kim JS *et al*. Efficacy and
498 safety of sorafenib in patients in the Asia-Pacific region with advanced
499 hepatocellular carcinoma: a phase III randomised, double-blind,
500 placebo-controlled trial. *The Lancet Oncology* 2009; **10**: 25–34.
- 501 4 Raoul J-L, Kudo M, Finn RS, Edeline J, Reig M, Galle PR. Systemic
502 therapy for intermediate and advanced hepatocellular carcinoma: Sorafenib
503 and beyond. *Cancer Treatment Reviews* 2018; **68**: 16–24.
- 504 5 Dixon SJ, Lemberg KM, Lamprecht MR, Skouta R, Zaitsev EM, Gleason
505 CE *et al*. Ferroptosis: An Iron-Dependent Form of Nonapoptotic Cell Death.
506 *Cell* 2012; **149**: 1060–1072.
- 507 6 Stockwell BR, Friedmann Angeli JP, Bayir H, Bush AI, Conrad M, Dixon SJ
508 *et al*. Ferroptosis: A Regulated Cell Death Nexus Linking Metabolism, Redox
509 Biology, and Disease. *Cell* 2017; **171**: 273–285.

- 510 7 Forcina GC, Dixon SJ. GPX4 at the Crossroads of Lipid Homeostasis and
511 Ferroptosis. *Proteomics* 2019; **19**: 1800311.
- 512 8 Lei P, Bai T, Sun Y. Mechanisms of Ferroptosis and Relations With
513 Regulated Cell Death: A Review. *Front Physiol* 2019; **10**: 139.
- 514 9 Nie J, Lin B, Zhou M, Wu L, Zheng T. Role of ferroptosis in hepatocellular
515 carcinoma. *J Cancer Res Clin Oncol* 2018; **144**: 2329–2337.
- 516 10 Lachaier E, Louandre C, Godin C, Saidak Z, Baert M, Diouf M *et al.*
517 Sorafenib Induces Ferroptosis in Human Cancer Cell Lines Originating from
518 Different Solid Tumors. *Anticancer Res* 2014; **34**: 6417-6422.
- 519 11 Louandre C, Ezzoukhry Z, Godin C, Barbare J-C, Mazière J-C, Chauffert B
520 *et al.* Iron-dependent cell death of hepatocellular carcinoma cells exposed to
521 sorafenib: Iron-dependent cytotoxicity of sorafenib. *Int J Cancer* 2013; **133**:
522 1732–1742.
- 523 12 Townsend DM, Tew KD. The role of glutathione-S-transferase in
524 anti-cancer drug resistance. *Oncogene* 2003; **22**: 7369–7375.
- 525 13 Zhang J, Ye Z, Chen W, Culpepper J, Jiang H, Ball LE *et al.* Altered redox
526 regulation and S-glutathionylation of BiP contribute to bortezomib resistance in
527 multiple myeloma. *Free Radical Biology and Medicine* 2020; **160**: 755–767.
- 528 14 Henderson CJ, McLaren AW, Wolf CR. In Vivo Regulation of Human
529 Glutathione Transferase GSTP by Chemopreventive Agents. *Cancer Res*.
530 2014; **74**: 4378-4387.
- 531 15 Wang X, Huang ZH. Predictive potential role of glutathione S-transferase

- 532 polymorphisms in the prognosis of breast cancer. *Genet Mol Res* 2015; **14**:
533 10236–10241.
- 534 16 Tew KD. Glutathione-Associated Enzymes In Anticancer Drug Resistance.
535 *Cancer Research* 2016; **76**: 7–9.
- 536 17 Rocha G da G, Oliveira RR, Kaplan MAC, Gattass CR. 3 β -Acetyl tormentic
537 acid reverts MRP1/ABCC1 mediated cancer resistance through modulation of
538 intracellular levels of GSH and inhibition of GST activity. *European Journal of
539 Pharmacology* 2014; **741**: 140–149.
- 540 18 Fernández-Cañón JM, Peñalva MA. Characterization of a Fungal
541 Maleylacetoacetate Isomerase Gene and Identification of Its Human
542 Homologue. *J Biol Chem* 1998; **273**: 329–337.
- 543 19 Yang F, Li J, Deng H, Wang Y, Lei C, Wang Q *et al.* GSTZ1-1 Deficiency
544 Activates NRF2/IGF1R Axis in HCC via Accumulation of Oncometabolite
545 Succinylacetone. *EMBO J* 2019; **38**. doi:10.15252/embj.2019101964.
- 546 20 Li J, Wang Q, Yang Y, Lei C, Yang F, Liang L *et al.* GSTZ1 deficiency
547 promotes hepatocellular carcinoma proliferation via activation of the
548 KEAP1/NRF2 pathway. *J Exp Clin Cancer Res* 2019; **38**: 438.
- 549 21 van Malenstein H, Dekervel J, Verslype C, Van Cutsem E, Windmolders P,
550 Nevens F *et al.* Long-term exposure to sorafenib of liver cancer cells induces
551 resistance with epithelial-to-mesenchymal transition, increased invasion and
552 risk of rebound growth. *Cancer Letters* 2013; **329**: 74–83.
- 553 22 Ye Z, Hu Q, Zhuo Q, Zhu Y, Fan G, Liu M *et al.* Abrogation of ARF6

- 554 promotes RSL3-induced ferroptosis and mitigates gemcitabine resistance in
555 pancreatic cancer cells. *Am J Cancer Res.* 2020; **10**: 1182-1193.
- 556 23 Li Y, Yan H, Xu X, Liu H, Wu C, Zhao L. Erastin/sorafenib induces cisplatin
557 -resistant non-small cell lung cancer cell ferroptosis through inhibition of the
558 Nrf2/xCT pathway. *Oncol Lett.* 2020; **19**: 323-333.
- 559 24 Sun X, Niu X, Chen R, He W, Chen D, Kang R *et al.* Metallothionein-1G
560 facilitates sorafenib resistance through inhibition of ferroptosis. *Hepatology*
561 2016; **64**: 488–500.
- 562 25 Dixon SJ, Patel DN, Welsch M, Skouta R, Lee ED, Hayano M *et al.*
563 Pharmacological inhibition of cystine–glutamate exchange induces
564 endoplasmic reticulum stress and ferroptosis. *eLife* 2014; **3**: e02523.
- 565 26 Sun X, Ou Z, Chen R, Niu X, Chen D, Kang R *et al.* Activation of the
566 p62-Keap1-NRF2 pathway protects against ferroptosis in hepatocellular
567 carcinoma cells: Hepatobiliary Malignancies. *Hepatology* 2016; **63**: 173–184.
- 568 27 Li D, Li Y. The interaction between ferroptosis and lipid metabolism in
569 cancer. *Sig Transduct Target Ther* 2020; **5**: 108.
- 570 28 Kobayashi A, Kang M-I, Okawa H, Ohtsuji M, Zenke Y, Chiba T *et al.*
571 Oxidative Stress Sensor Keap1 Functions as an Adaptor for Cul3-Based E3
572 Ligase To Regulate Proteasomal Degradation of Nrf2. *MCB* 2004; **24**:
573 7130–7139.
- 574 29 Dai C, Chen X, Li J, Comish P, Kang R, Tang D. Transcription factors in
575 ferroptotic cell death. *Cancer Gene Ther* 2020; **27**: 645–656.

- 576 30 Dodson M, Castro-Portuguez R, Zhang DD. NRF2 plays a critical role in
577 mitigating lipid peroxidation and ferroptosis. *Redox Biology* 2019; **23**: 101107.
- 578 31 Venook AP, Papandreou C, Furuse J, Ladrón de Guevara L. The Incidence
579 and Epidemiology of Hepatocellular Carcinoma: A Global and Regional
580 Perspective. *The Oncologist* 2010; **15**: 5–13.
- 581 32 Llovet JM, Montal R, Sia D, Finn RS. Molecular therapies and precision
582 medicine for hepatocellular carcinoma. *Nat Rev Clin Oncol* 2018; **15**: 599–616.
- 583 33 Townsend DM, Tew KD. The role of glutathione-S-transferase in
584 anti-cancer drug resistance. *Oncogene* 2003; **22**: 7369–7375.
- 585 34 Tew KD. Glutathione-Associated Enzymes In Anticancer Drug Resistance.
586 *Cancer Research* 2016; **76**: 7–9.
- 587 35 Pereira D, Assis J, Gomes M, Nogueira A, Medeiros R. Improvement of a
588 predictive model in ovarian cancer patients submitted to platinum-based
589 chemotherapy: implications of a GST activity profile. *Eur J Clin Pharmacol*
590 2016; **72**: 545–553.
- 591 36 Sawers L, Ferguson MJ, Ihrig BR, Young HC, Chakravarty P, Wolf CR *et al.*
592 Glutathione S-transferase P1 (GSTP1) directly influences platinum drug
593 chemosensitivity in ovarian tumour cell lines. *Br J Cancer* 2014; **111**:
594 1150–1158.
- 595 37 Singh RR, Mohammad J, Orr M, Reindl KM. Glutathione S-Transferase
596 pi-1 Knockdown Reduces Pancreatic Ductal Adenocarcinoma Growth by
597 Activating Oxidative Stress Response Pathways. *Cancers (Basel)* 2020; **12**:

- 598 1501.
- 599 38 Tong X, Zhao J, Zhang Y, Mu P, Wang X. Expression levels of MRP1,
600 GST- π , and GSK3 β in ovarian cancer and the relationship with drug resistance
601 and prognosis of patients. *Oncol Lett.* 2019; **18**: 22-28.
- 602 39 Wang Q. Expression of P-gp, MRP, LRP, GST- π and Topolla and intrinsic
603 resistance in human lung cancer cell lines. *Oncol Rep.* 2011; **26**: 1081-1089.
- 604 40 Zou M, Hu X, Xu B, Tong T, Jing Y, Xi L et al. Glutathione S-transferase
605 isozyme alpha 1 is predominantly involved in the cisplatin resistance of
606 common types of solid cancer. *Oncol Rep* 2019; **41**: 989–998.
- 607 41 Manz DH, Blanchette NL, Paul BT, Torti FM, Torti SV. Iron and cancer:
608 recent insights: Iron and cancer. *Ann NY Acad Sci* 2016; **1368**: 149–161.
- 609 42 Torti SV, Torti FM. Iron and cancer: more ore to be mined. *Nat Rev Cancer*
610 2013; **13**: 342–355.
- 611 43 Hassannia B, Vandenabeele P, Vanden Berghe T. Targeting Ferroptosis to
612 Iron Out Cancer. *Cancer Cell* 2019; **35**: 830–849.
- 613 44 Friedmann Angeli JP, Krysko DV, Conrad M. Ferroptosis at the crossroads
614 of cancer-acquired drug resistance and immune evasion. *Nat Rev Cancer*
615 2019; **19**: 405–414.
- 616 45 Yu Y, Xie Y, Cao L, Yang L, Yang M, Lotze MT et al. The ferroptosis inducer
617 erastin enhances sensitivity of acute myeloid leukemia cells to
618 chemotherapeutic agents. *Molecular & Cellular Oncology* 2015; **2**: e1054549.
- 619 46 Sato M, Kusumi R, Hamashima S, Kobayashi S, Sasaki S, Komiyama Y, et

- 620 *al.* The ferroptosis inducer erastin irreversibly inhibits system xc- and
621 synergizes with cisplatin to increase cisplatin's cytotoxicity in cancer cells. *Sci
622 Rep.* 2018; **8**: 968.
- 623 47 Bai T, Wang S, Zhao Y, Zhu R, Wang W, Sun Y. Haloperidol, a sigma
624 receptor 1 antagonist, promotes ferroptosis in hepatocellular carcinoma cells.
625 *Biochem Biophys Res Commun.* 2017; **491**: 919-925.
- 626 48 Shimada K, Skouta R, Kaplan A, Yang WS, Hayano M, Dixon SJ *et al.*
627 Global survey of cell death mechanisms reveals metabolic regulation of
628 ferroptosis. *Nat Chem Biol* 2016; **12**: 497–503.
- 629 49 Shimada K, Hayano M, Pagano NC, Stockwell BR. Cell-Line Selectivity
630 Improves the Predictive Power of Pharmacogenomic Analyses and Helps
631 Identify NADPH as Biomarker for Ferroptosis Sensitivity. *Cell Chemical
632 Biology* 2016; **23**: 225–235.
- 633 50 Bogdan AR, Miyazawa M, Hashimoto K, Tsuji Y. Regulators of Iron
634 Homeostasis: New Players in Metabolism, Cell Death, and Disease. *Trends in
635 Biochemical Sciences* 2016; **41**: 274–286.
- 636 51 Anandhan A, Dodson M, Schmidlin CJ, Liu P, Zhang DD. Breakdown of an
637 Ironclad Defense System: The Critical Role of NRF2 in Mediating Ferroptosis.
638 *Cell Chemical Biology* 2020; **27**: 436–447.
- 639
- 640

641 **Acknowledgements**

642 We wish to thank Dr. T.-C He (University of Chicago, USA) for providing the
643 plasmids pAdEasy system, and Prof. Ding Xue (Tsinghua University) for
644 supplying the CRISPR/Cas9 system.

645

646 **Conflict of interest**

647 The authors declare that they have no conflict of interest.

648

649 **Authors' contributions**

650 ALH, NT and KW conceived the study and designed the experiments. QJW,
651 BC and QX performed most experiments and analyzed the data. QZG assisted
652 with experiments in *Gstz1*^{-/-} knockout mice. QJW, NT and KW drafted and
653 edited the manuscript with all authors providing feedback.

654

655 **Ethics Statement**

656 This study was approved by the Research Ethics Committee of Chongqing
657 Medical University (reference number: 2017010).

658

659 **Funding**

660 This work was supported by the China National Natural Science Foundation
661 (grant no. 81872270, 82072286, 82073251), the Natural Science Foundation
662 Project of Chongqing (cstc2018jcyjAX0254, cstc2019jcyj-msxmX0587), the

663 Major National S&T program (2017ZX10202203-004), the Scientific Research
664 Innovation Project for Postgraduate in Chongqing (grant no. CYS19192), and
665 the Science and Technology Research Program of Chongqing Municipal
666 Education Commission (KJZD-M202000401, KJQN201900429).

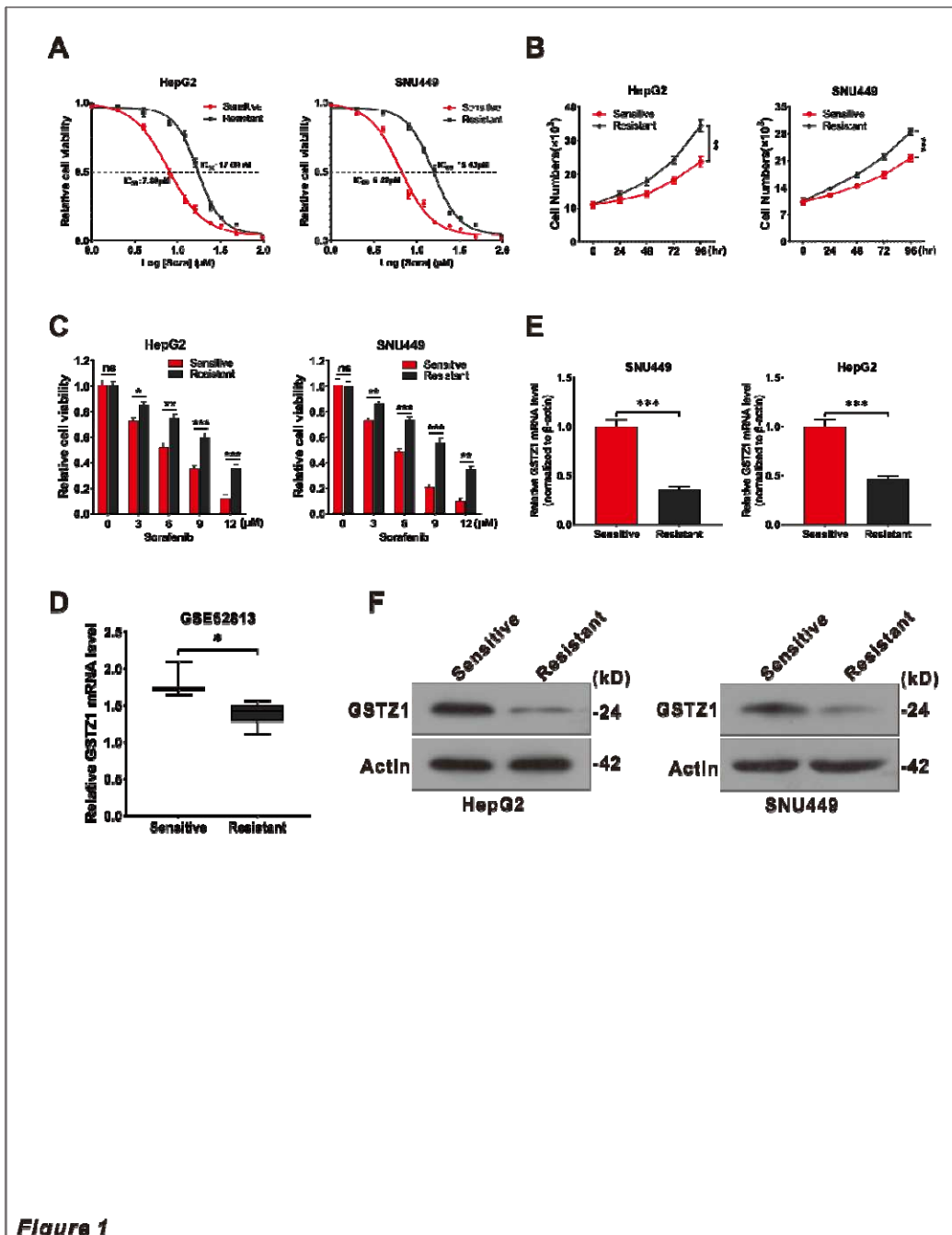
667

668 **Data Availability**

669 The datasets used and/or analyzed during the current study are available from
670 the corresponding author on reasonable request.

671

672 **Figures and figure legends**

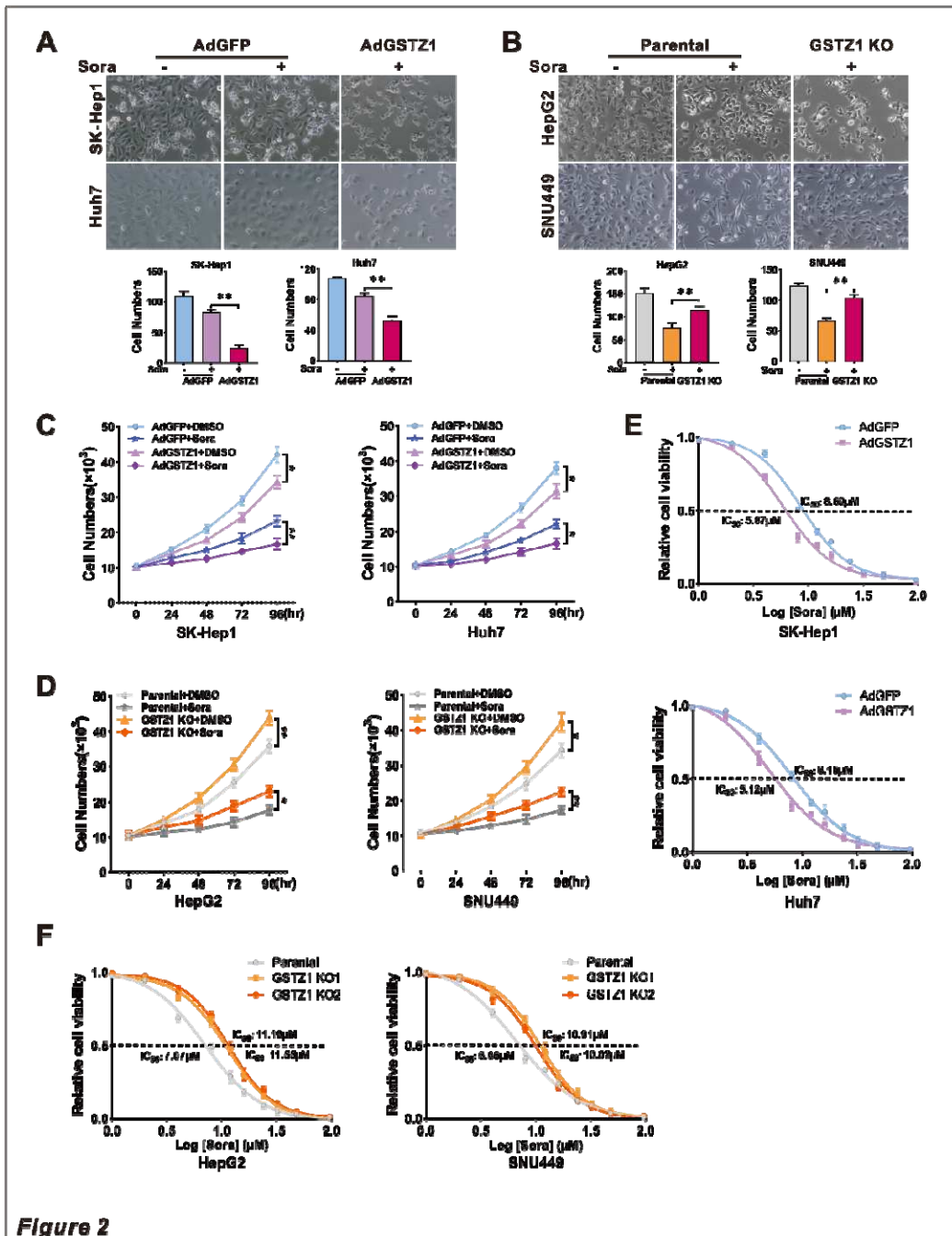


673 **Figure 1**

674 **Fig. 1** GSTZ1 is downregulated in sorafenib-resistant HCC cells. **a** The IC₅₀
675 values of sorafenib-sensitive and sorafenib-resistant HCC cells treated with
676 sorafenib. **b** Cell growth curve. **c** These sorafenib-sensitive and

677 sorafenib-resistant HCCs (HepG2, SNU449) were treated with indicated
678 concentrations of sorafenib for 24 h, and cell viability was assayed using the
679 CCK-8 assay. **d** GSTZ1 RNA level in sorafenib-sensitive HepG2 cells (n=3)
680 and sorafenib-resistant HepG2 cells (n=10). **e-f** mRNA and protein levels of
681 GSTZ1 in sorafenib-sensitive and sorafenib-resistant cells. For Western
682 blotting, 50 µg protein was loaded per well. HCC: hepatocellular carcinoma.
683 Values represent the mean \pm standard deviation (SD) (n = 3, performed in
684 triplicate). ns: no significant difference, *p < 0.05, **p < 0.01, ***p < 0.001,
685 Student's *t*-test (two groups) or one-way ANOVA followed by Tukey tests (three
686 groups).

687



688

689 **Fig. 2** GSTZ1 knockout promotes sorafenib resistance in HCC cells. **a-b**

690

690 Morphological phase-contrast images (top) and quantification (bottom) of cells
691 after treatment with or without sorafenib (10 μ M) for 24 h. Magnifications: $\times 200$.

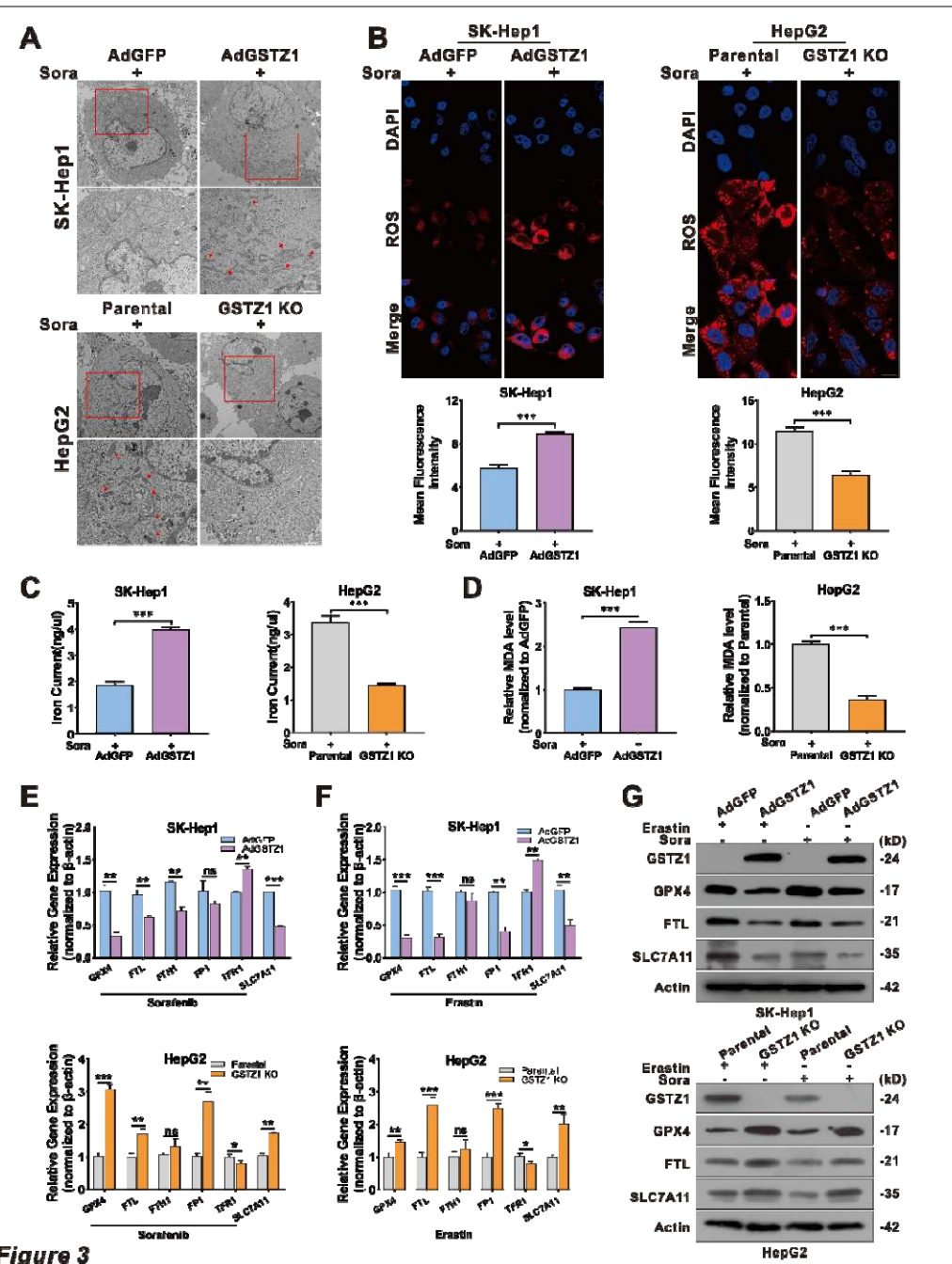
692

692 **c-d** Cell growth curve. GSTZ1 overexpression (OE) (**c**) and GSTZ1 knockout

693 (KO) (**d**) cells were treated with or without sorafenib (10 μ M). **e-f** The IC50 of
694 GSTZ1-OE (**g**) and GSTZ1-KO (**h**) cells were determined using the CCK-8
695 assay. HCC: hepatocellular carcinoma, DMSO: dimethyl sulphoxide, Sora:
696 sorafenib. Values represent the mean \pm SD (n = 3, performed in triplicate). *p <
697 0.05, **p < 0.01, Student's t-test (two groups) or one-way ANOVA followed by
698 Tukey tests (three groups).

699

700



701

Figure 3

702 **Fig. 3** GSTZ1 overexpression enhances sorafenib-induced ferroptosis in HCC.

703 **a** Representative TEM images of the mitochondrial morphology in GSTZ1-OE

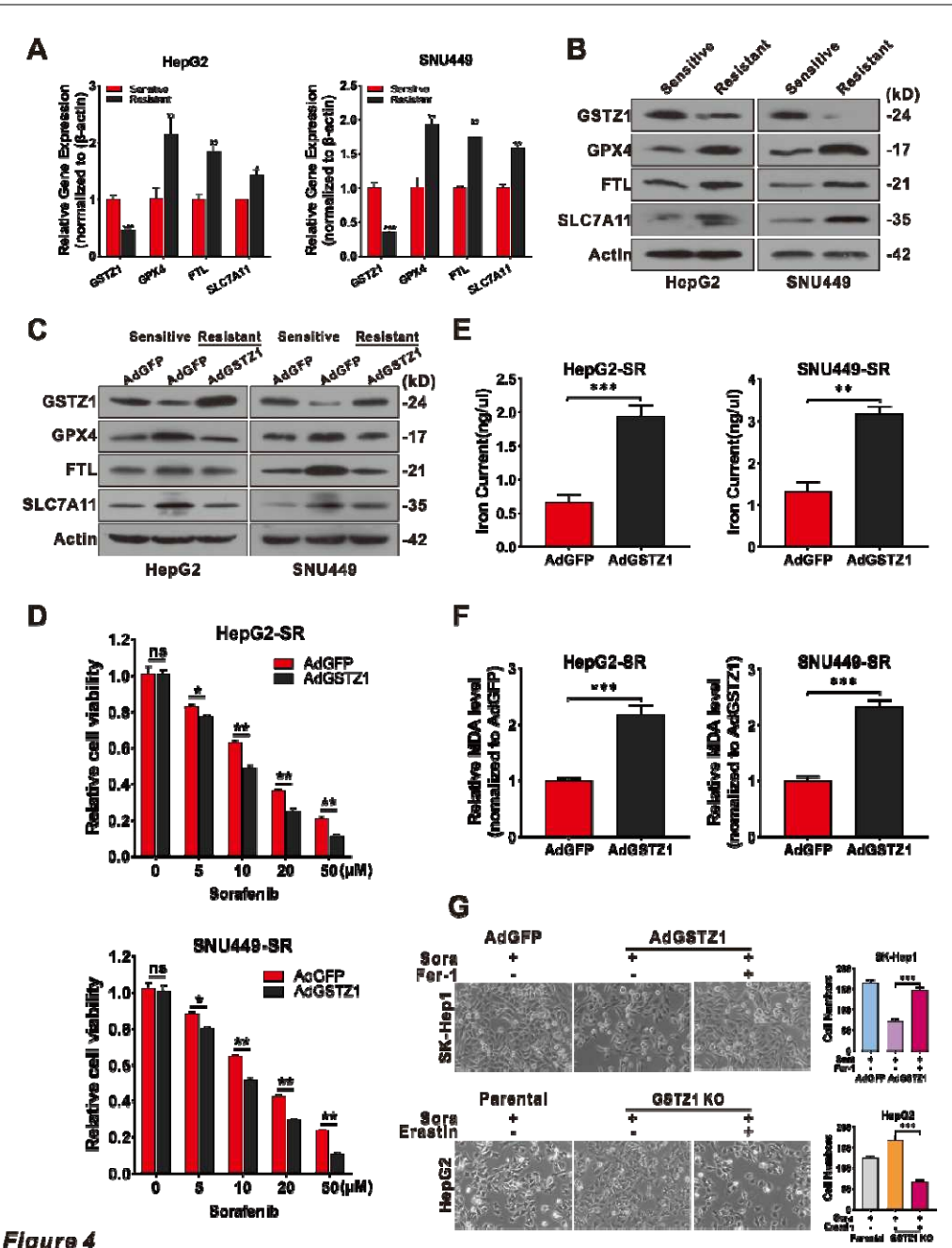
704 SK-Hep1 and GSTZ1-KO HepG2 cells treated with 10 μM sorafenib for 24 h.

705 Red arrows indicate mitochondria. Bar = 1 μm. **b** Representative images (top)

706 and quantification (bottom) of ROS level in GSTZ1-OE and GSTZ1-KO cells
707 treated with sorafenib for 24 h. Bar = 20 μ m. **c-d** The intracellular iron (**c**) and
708 MDA (**d**) levels in GSTZ1-OE and GSTZ1-KO cells treated with sorafenib for
709 24 h. **e-g** mRNA and protein levels of target genes associated with ferroptosis
710 in GSTZ1-OE and GSTZ1-KO cells treated with sorafenib or erastin,
711 determined via qRT-PCR (**e-f**) and Western blotting (**g**), respectively. For
712 Western blotting, 50 μ g protein was loaded per well. HCC: hepatocellular
713 carcinoma, Sora: sorafenib, ROS: reactive oxygen species, MDA:
714 malondialdehyde. Values represent the mean \pm SD (n = 3, performed in
715 triplicate). ns: no significant difference, *p < 0.05, **p < 0.01, ***p < 0.001,
716 Student's *t*-test (two groups) or one-way ANOVA followed by Tukey tests (three
717 groups).

718

719



720

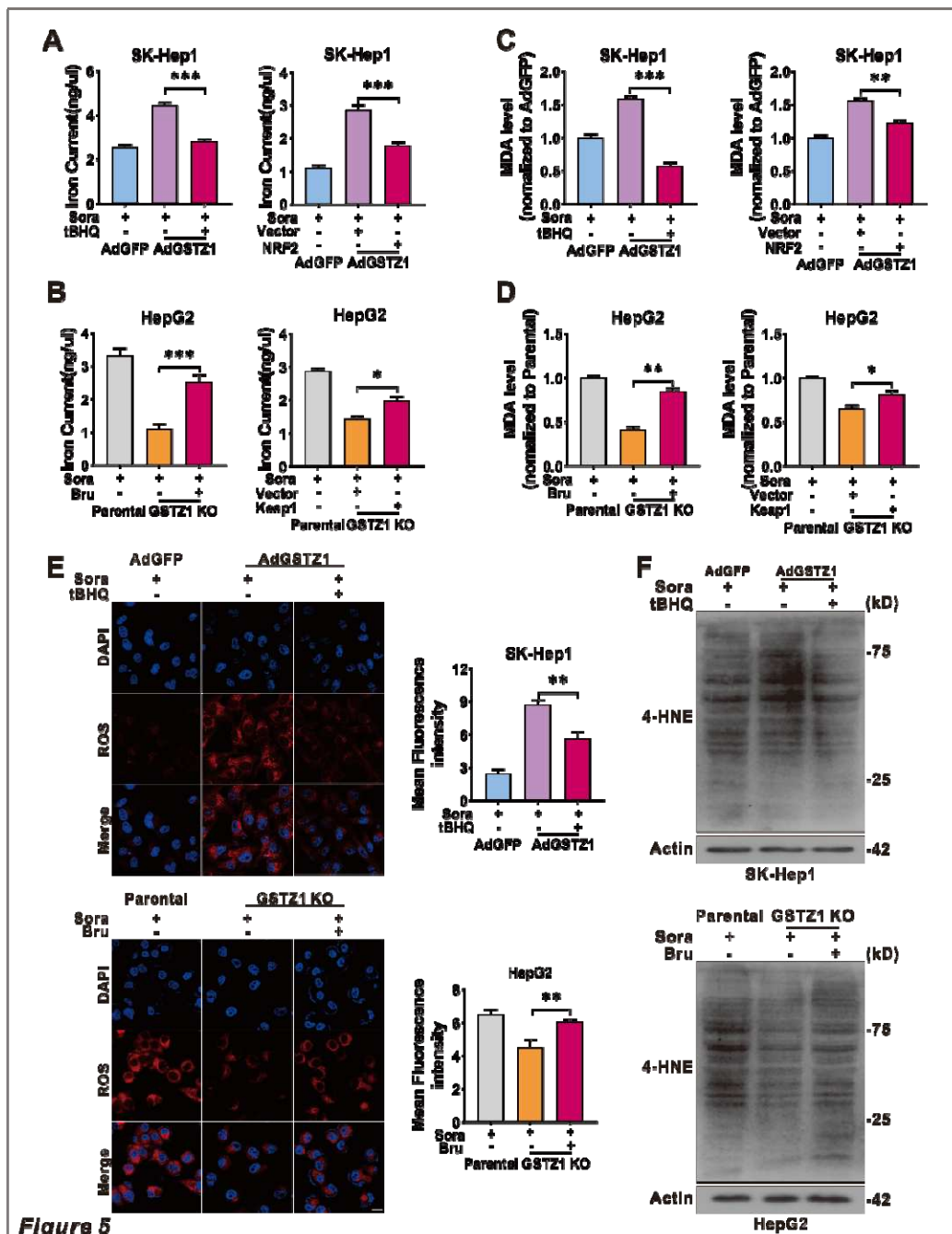
Figure 4

721 **Fig. 4** GSTZ1 overexpression sensitizes hepatoma cells to sorafenib-induced
 722 ferroptosis. **a-b** The mRNA (**a**) and protein (**b**) levels of ferroptosis-related
 723 genes in sorafenib-sensitive and sorafenib-resistant cells were assayed using
 724 qRT-PCR and Western blotting, respectively. **c** Western blotting for

725 assessment of protein levels of ferroptosis-related genes in sorafenib-resistant
726 HCCs with adenoviruses expressing GFP (AdGFP) or GSTZ1 (AdGSTZ1). **d**
727 The cell viability of sorafenib-resistant cell with GSTZ1 overexpression was
728 determined using CCK-8 assay. **e-f** The iron (**e**) and MDA (**f**) levels in
729 GSTZ1-OE sorafenib-resistant cells. **g** The morphology (left) and
730 quantification (right) of indicated HCC cells treated with sorafenib (10 μ M for
731 24 h) alone or in combination with Fer-1 (1 μ M for 24 h) or erastin (10 μ M for
732 24 h). Magnifications: $\times 200$. For Western blotting, 50 μ g protein was loaded
733 per well. HCC: hepatocellular carcinoma, Sora: sorafenib, MDA:
734 malondialdehyde, Fer-1: ferrostatin-1, SR: sorafenib resistant. Values
735 represent the mean \pm SD (n = 3, performed in triplicate). ns: no significant
736 difference, *p < 0.05, **p < 0.01, ***p < 0.001, Student's t-test (two groups) or
737 one-way ANOVA followed by Tukey tests (three groups).

738

739



740

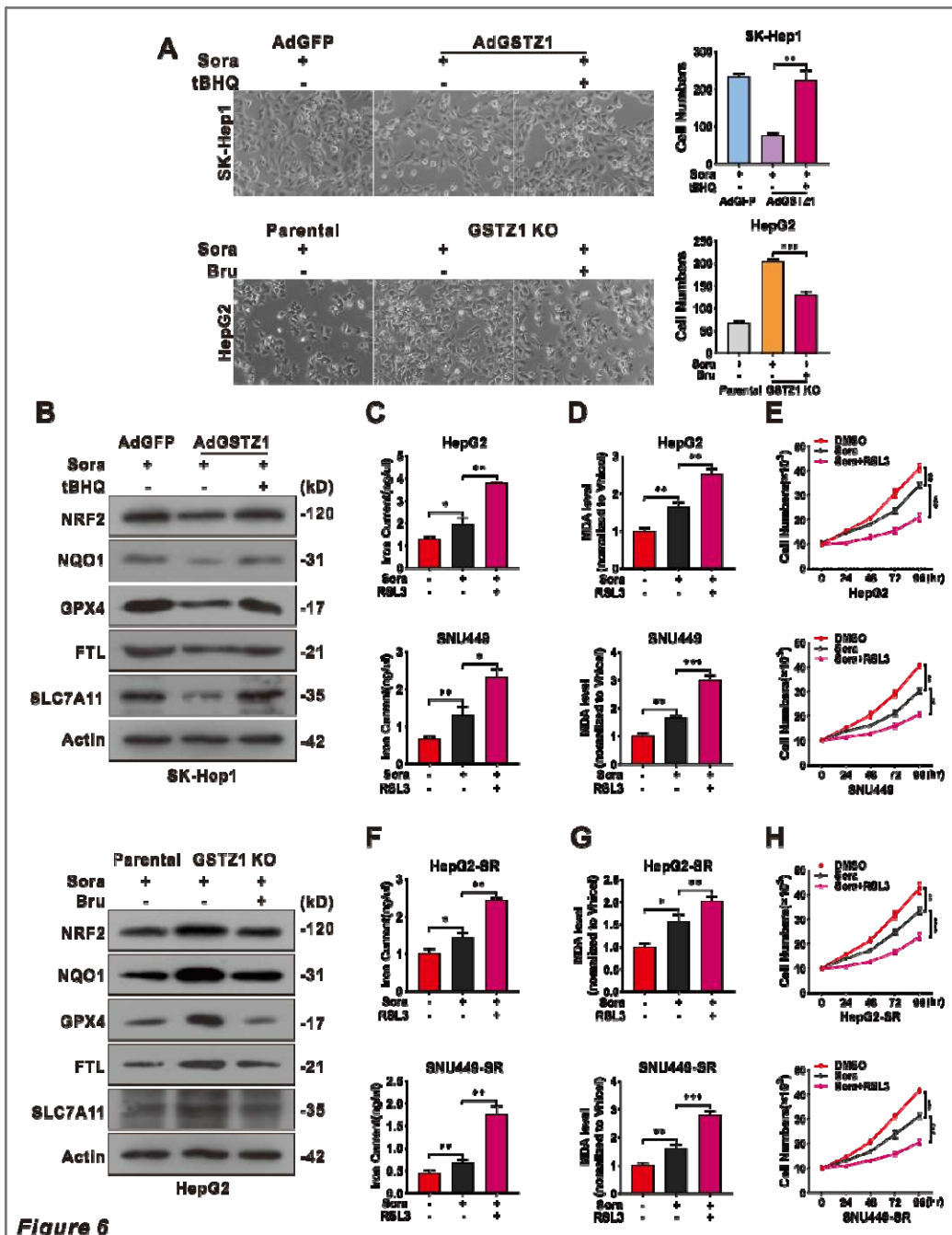
Figure 5

741 **Fig. 5** GSTZ1 knockout cells are insensitive to sorafenib-induced ferroptosis
 742 through the activation of NRF2. **a** GSTZ1-OE cells were treated with sorafenib
 743 alone or in combination with tBHQ (100 μ M for 3 h) (left). GSTZ1-KO cells
 744 were treated with sorafenib alone or in combination with Bru (40 nM for 24 h)

745 (left). Expressing Flag-KEAP1 plasmid was transfected into GSTZ1-OE cells
746 with sorafenib treatment (right). Expressing Myc-NRF2 plasmid was
747 transfected into GSTZ1-KO cells with sorafenib treatment (right). Levels of iron
748 (**a-b**), and MDA (**c-d**) in these cells were assayed. **e** Representative images
749 (top) and quantification (bottom) of ROS level in GSTZ1-OE cells treated with
750 sorafenib alone or in combination with tBHQ (top) and GSTZ1-KO cells treated
751 with sorafenib alone or in combination with Bru (bottom). Bar = 20 μ m. **f**
752 4-HNE-induced protein modification were examined. The cell processing is
753 described as above. For Western blotting, 50 μ g protein was loaded per well.
754 tBHQ: tertiary butylhydroquinone, Bru: brusatol, Sora: sorafenib, MDA:
755 malondialdehyde, 4-HNE: 4-hydroxy-2-nonenal. Values represent the mean \pm
756 SD (n = 3, performed in triplicate). ns: no significant difference, *p < 0.05, **p <
757 0.01, ***p < 0.001, Student's t-test (two groups) or one-way ANOVA followed
758 by Tukey tests (three groups).

759

760



761

762 **Fig. 6** RSL3 enhances the sensitivity of GSTZ1-KO and sorafenib-resistant
 763 cells to sorafenib. **a-b** Morphological changes (**a**) and protein level (**b**) of
 764 ferroptosis-related genes in GSTZ1-OE SK-Hep1 cells treated with sorafenib
 765 alone or in combination with tBHQ (top) and GSTZ1-KO HepG2 cells treated

766 with sorafenib alone or in combination with Bru (bottom). Magnifications: $\times 200$.

767 **c-d** The iron (left) and MDA (right) levels in GSTZ1-KO cells treated with

768 sorafenib alone or in combination with RSL3 (500nM for 24 h). **e** The cell

769 growth curve of GSTZ1-KO cells treated with sorafenib alone or in combination

770 with RSL3. **f-g** The iron (left) and MDA (right) levels in sorafenib-resistant cells

771 treated with sorafenib alone or in combination with RSL3. **h** The cell growth

772 curve of sorafenib-resistant cells treated with sorafenib alone or in combination

773 with RSL3. For Western blotting, 50 μ g protein was loaded per well. RSL3:

774 Ras-selective lethal small molecule 3, tBHQ: tertiary butylhydroquinone, Bru:

775 brusatol, DMSO: dimethyl sulphoxide, Sora: sorafenib, MDA: malondialdehyde.

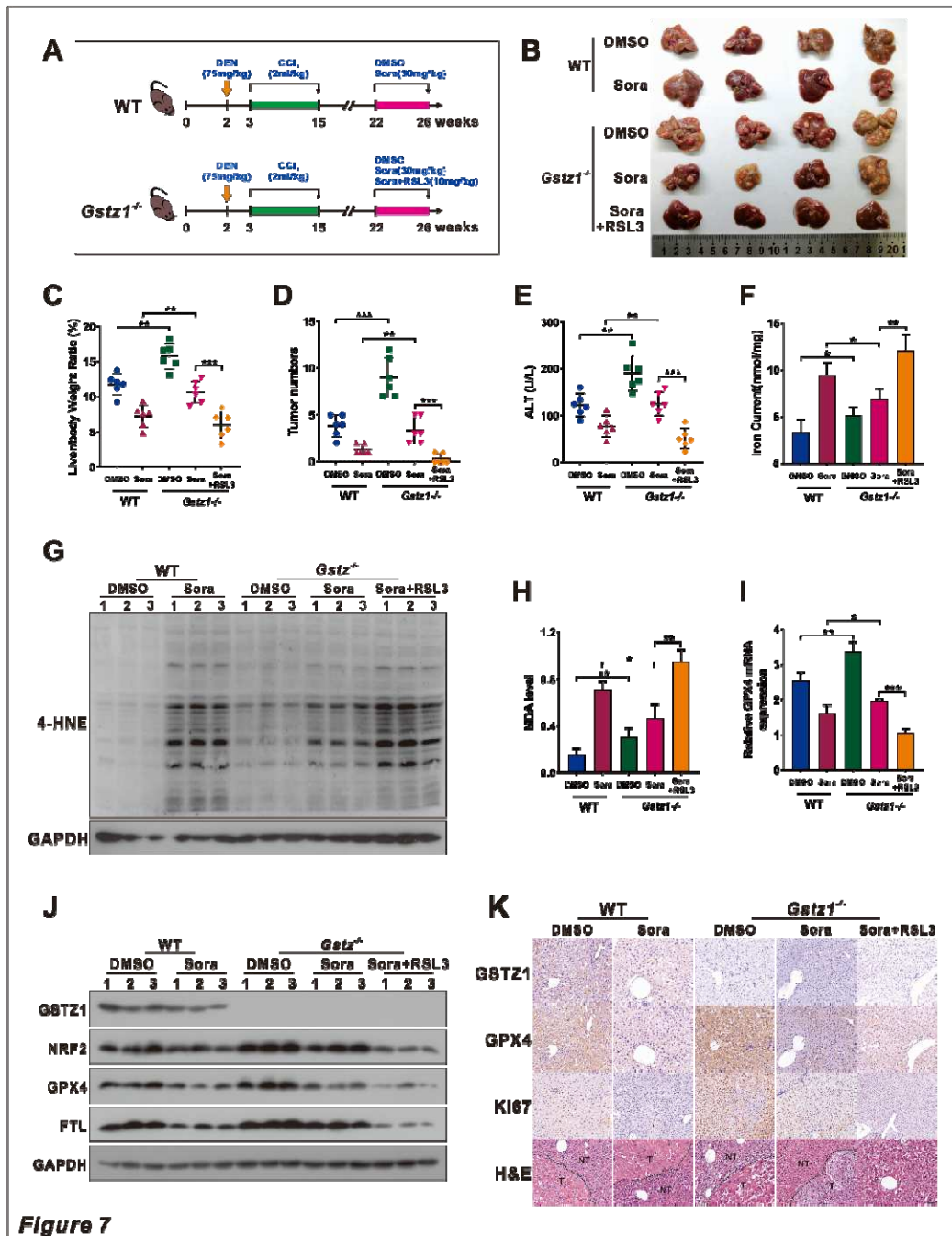
776 Values represent the mean \pm SD (n = 3, performed in triplicate). *p < 0.05, **p

777 < 0.01, ***p < 0.001, Student's t-test (two groups) or one-way ANOVA followed

778 by Tukey tests (three groups).

779

780



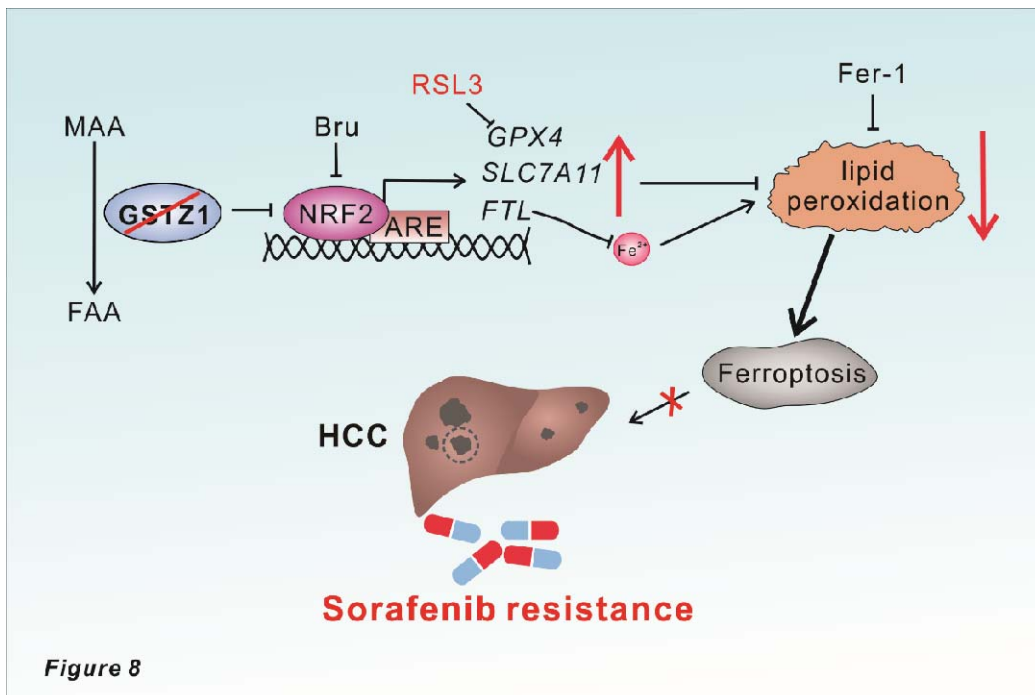
781 **Figure 7**

782 **Fig. 7** RSL3 enhances the anticancer activity of sorafenib in *Gstz1*^{-/-} mice. **a**
783 Schematic representation of the experimental design for mice. **b** Gross
784 appearances of liver tumors. The red circles represent tumors. **c-e** In vivo
785 analyses of liver/body weight ratio (**c**), tumor numbers (**d**), and serum alanine

786 aminotransferase (ALT) (**e**) levels of the five groups. **f-h** The levels of iron (**f**)
787 and MDA (**h**) in mice were assayed. Western blotting to assess 4-HNE
788 modification level (**g**) in murine livers. **i-j** mRNA (**i**) and protein (**j**) levels of
789 GPX4, FTL, and SLC7A11 in the five groups of liver tumors as assessed using
790 Western blotting and real-time qPCR, respectively. **k** Representative H&E
791 staining and immunohistochemistry images of GSTZ1, GPX4, and Ki67 in
792 hepatic tumors. Bar = 50 μ m. For Western blotting, 50 μ g protein was loaded
793 per well. WT: wild type, DEN: diethylnitrosamine, CCl₄: carbon tetrachloride,
794 DMSO: dimethyl sulphoxide, Sora: sorafenib, RSL3: Ras-selective lethal small
795 molecule 3, ALT: alanine aminotransferase, 4-HNE: 4-hydroxy-2-nonenal, H&E:
796 hematoxylin and eosin. Values represent the mean \pm SD (n = 3, performed in
797 triplicate). *p < 0.05, **p < 0.01, ***p < 0.001, Student's t-test (two groups) or
798 one-way ANOVA followed by Tukey tests (five groups).

799

800



801

802 **Fig. 8** A proposed model of the resistance of GSTZ1-deficient cells to
803 sorafenib. MAA: maleylacetoacetate, FAA: fumarylacetoacetate, Bru: brusatol,
804 ARE: anti-oxidation response element. Fer-1: ferrostatin-1, HCC:
805 hepatocellular carcinoma.